Hindawi
Advances in Civil Engineering
Volume 2019, Article ID 7696752, 19 pages
https://doi.org/10.1155/2019/7696752

Research Article

Research on Physical Similarity Simulation of Mining Uphill and Downhill at the Large-Angle Working Face

Meng Zhang,[1,2] **Yidong Zhang**,[2] **Ming Ji**,[1,2] **Hongjun Guo**,[1,2] **and Haizhu Li**[1,2]

[1]*School of Mines, Key Laboratory of Deep Coal Resource Mining, Ministry of Education of China, China University of Mining and Technology, Xuzhou 221116, China*
[2]*State Key Laboratory of Coal Resources and Mine Safety, China University of Mining and Technology, Xuzhou 221116, China*

Correspondence should be addressed to Yidong Zhang; ydzhang@cumt.edu.cn

Received 21 September 2018; Revised 15 December 2018; Accepted 8 January 2019; Published 3 February 2019

Guest Editor: Ray R. Zhang

With the development of coal mining and the continuous expansion of mining intensity, large dip angle comprehensive mechanized coal mining as an important development direction and goal has become a worldwide research topic in the coal industry. The working face faces many production problems that need to be solved, such as the large-angle downhill mining, the large-angle uphill mining, and other complicated geological conditions (such as skew, anticline, and fault). In view of the above problems, with the specific conditions of Xinji No. 2 Mine, through the physical similarity simulation, the research on the roof movement law of the fully mechanized mining face under the mining conditions of large dip angle (depression angle and elevation angle are more than 40° and 20°, respectively) is studied. The distribution law of abutment pressure, movement law, and distribution range of water-conducting fracture zone after mining are emphasized. Meanwhile, the paper analyzes and compares the related mining pressure law of inclined longwall fully mechanized mining face under general conditions, forming a systematic, comprehensive, and scientific understanding of the law of mining pressure under such conditions. This achievement is of great significance to the prevention and control of water, support design, safety production, environmental improvement, improvement of enterprise efficiency, and advancement of coal science and technology.

1. Introduction

1.1. Purpose and Significance of the Research. Mine pressure refers to the force formed in the surrounding rock mass of roadway and chamber, acting on its support due to the influence of mining activities. It is also called secondary stress or engineering disturbance force in related disciplines. After excavating roadways in rock mass, the stress redistribution will inevitably occur in the surrounding rock of roadways. In general, the increased tangential stress on both sides of the roadway is called abutment pressure. After a coal seam is mined, the original stress balance state around the goaf is destroyed, resulting in the redistribution of stress, deformation, destruction, and movement of rock strata, and mine pressure will further lead to the movement and subsidence of strata and gradually develop to the upper strata, which will eventually lead to surface movement and subsidence. This process and phenomenon is called the movement of overlying strata. In some mines with long mining time or complicated geological conditions, with the increase of mining intensity and years, the reserves of working face that meet the conditions of conventional fully mechanized mining are gradually reduced or even depleted [1–5]. Among the remaining reserves of blocks and coal pillars, there are more complicated geological conditions with a large dip angle coal seam. The current development level of coal seam mining with a large dip angle (including strike angle) is much lower than that of gently inclined coal seam, and there are a series of unsolved basic technical problems. Therefore, it is very necessary and urgent to study the mining method of a large dip angle coal seam (including strike angle).

The overall situation of coal mining in China is to transfer to the west. More than 50% of the coal mines in the west are mining large dip angle coal seams, such as Sichuan, Chongqing, Yunnan, Guizhou, Xinjiang, Gansu, and Ningxia, in major coal-producing provinces (districts). Large dip angle coal seams are the main coal seams in many mining areas or mines in the west of China; the second trend

is the transfer of coal mining to deep areas. With the depletion of coal resources in the central and eastern regions, coal mining is gradually shifting to the deep and complicated geological structure areas, the production conditions are deteriorating, the coal seam dip is enlarged, and the large dip angle coal seams, especially local large dip angle coal seam reserves, account for a large part [6–11]. Therefore, the research on the large dip angle fully mechanized mining technology under complicated conditions is carried out; the key technologies of roof mining management during large dip angle mining, especially the large-angle uphill and downhill mining, should be found, and the adaptability of the general fully mechanized mining equipment during large dip angle mining, especially the large-angle uphill and downhill mining, also should be studied, forming a complete set of the large-angle mechanized mining technology system. It is of great significance to improve the overall technical level of the large dip angle coal seam mining and promote the overall progress of the coal industry to set up a model of safe and efficient production mine under complicated conditions.

At present, for the mining of large dip angle working face, firstly, our understanding of the mining pressure law roof control theory and support design ideas are still on the basis of gently inclined coal seams; secondly, what kind of mine pressure law is presented is a lack of systematic and comprehensive understanding. With the increase of the dip angle of the working face, what is the particularity of roof collapse and caving law in coal seam mining? Under the above circumstances, compared with gently inclined coal seams, what are the differences between the immediate roof and the main roof in the distance of periodic roof pressure, the characteristics of periodic roof pressure, and the stress distribution characteristics of the hydraulic support? How can we effectively support the roof in these circumstances? How can we ensure the stability of the working face equipment? These are major issues related to production that need to be solved.

The E1108 working face of Xinji No. 2 Coal Mine has complex geological conditions, such as fold structure, large dip angle of the coal seam, and a maximum dip angle of 45°.The coal mining method is the pseudodownhill mining method in the inner section, the pseudouphill mining method in the outer section, the maximum downhill mining angle is 42°, and the maximum uphill mining angle is 25°, and more than ten faults are exposed in the working face. The poor production conditions in the working face will inevitably lead to the decline of advancing speed, resulting in the imbalance of mine production capacity. The geological conditions of the working face are extremely rare in the entire Huainan mining area, and the mine technology and management personnel have no experience in coal mining under such geological conditions. Therefore, in view of the above problems, under the specific conditions of Xinji No.2 Coal Mine, the roof movement law and roof weighting law of the fully mechanized mining face under the conditions of high dip angle (depression angle and elevation angle are more than 40° and 20°, respectively) are studied by physical similarity simulation so as to create conditions for high-efficiency mining of the working face.

1.2. Current Research Situations. As early as 1970s, the former Soviet Union conducted some research on the mining of large dip angle coal seams and studied various types of fully mechanized mining supports and coal mining machines used in mining uphill and downhill at the large-angle working face, which laid the basic scientific and technological foundation for coal seam mining. The proportion of comprehensive mechanized coal mining in countries outside China has reached 80–90% in the early twentieth century. Therefore, highly mechanized and automated mining methods and techniques are the development trend of coal mining. The research on mining technology uphill and downhill at the large-angle working face outside China is mainly focused on the mining equipment [12–19].

According to the published literature and achievements, the occurrence conditions of coal seam in countries outside China are relatively simple, and the research on large-angle fully mechanized mining technology is mainly focused on mining equipment [20–22]. There are few systematic studies on the mining theory and technology, and the level is not high. Overall, however, China has achieved some results in some mining areas through theoretical research and field practice. However, there are few systematic studies on mining theory and technology, and the level is not high. How to achieve efficient and safe mining on fully mechanized coal mining face under the conditions of pitching, tilting, and large-angle longwall mining face has its particularity in mining technology, and there is no successful precedent for achieving high productivity and high efficiency in coal mine enterprises at home and abroad. It can be said that the comprehensive safety support technology of mining uphill and downhill at the large-angle working face has not yet achieved real success in China, and the main reason is that the basic problems of fully mechanized mining technology in the large dip angle coal seam have not been completely solved.

The successful research of this subject can effectively utilize the core technology of fully mechanized coal mining to achieve high productivity and high efficiency in coal mine enterprises under complex geological conditions of large dip angle coal seams (including large-angle uphill and downhill mining) and has a good prospect of popularization and application.

2. Physical Simulation Experimental Program

2.1. Experimental Objective. The essence of the physical similar material simulation method is to make the model of the mine rock layer (within the scope of the study) with similar materials according to the similarity principle and then to "mine" the actual situation of coal seam simulation in the model, and to observe the movement, deformation, and destruction of rock strata caused by "mining" in the model. According to the displacement and deformation of the model, the deformation and failure of the rock strata in

the field are analyzed and deduced, and the stress distribution law of the surrounding rock is studied [23–27].

The main purpose of this experiment is as follows:

(1) Through the physical similarity simulation, the law of roof movement and the law of roof pressure in the large-angle fully mechanized working face under uphill and downhill mining are revealed, the roof movement law and the law of roof pressure in a generally inclined longwall fully mechanized working face are compared and analyzed, and the particularity of the roof activities in the large-angle fully mechanized working face is summarized

(2) Through the physical similarity simulation, the overlying strata activity law during the large-angle fully mechanized working face is revealed, and the water-conducting fracture zone is found out, which provides the basis for water prevention and control in working face

2.2. Experimental Principles

2.2.1. Similarity Theory. The success of similar simulation experiments often depends on the degree of satisfaction of the similar conditions of the model and the prototype. The similar simulation experiment is to use the material with similar mechanical properties as the prototype, simulate the rock mass and the vein according to a certain geometric ratio, and carry out the excavation. Under the similar boundary and initial conditions, it will cause the similar ground pressure phenomenon in the corresponding period of time. Through the measurement and analysis of its laws, the basis and improvement ways are put forward for improving excavation technology, preventing accidents and selecting mining methods. Similar conditions are observed when planning simulation tests. According to the requirements of general physical phenomena similarity, the following basic similar conditions should be met between the model ($''$) and the prototype ($'$):

(1) Geometric similarity:

$$\frac{l_1'}{l_1''} = \frac{l_2'}{l_2''} = \ldots = c_l. \tag{1}$$

(2) Kinematic similarity:

$$\frac{t_1'}{t_1''} = \frac{t_2'}{t_2''} = \ldots = c_t = \sqrt{c_l}. \tag{2}$$

(3) Stress similarity:

$$c_p = c_r \cdot c_l, \tag{3}$$

where c_r is the ratio of bulk density.

(4) Dynamic similarity:

$$F = m\frac{dv}{dt}. \tag{4}$$

From which we can derive $(m_1'/m_1'') = (m_2'/m_2'') = \ldots = c_m = c_r \cdot c_l^3$.

(5) External force similarity:

$$c_F = c_r \cdot c_l^3. \tag{5}$$

On the basis of satisfying the above conditions, the laying model and the location of ore veins in the model must also satisfy the similarity of boundary conditions. The uniaxial compressive strength indexes of similar simulated materials and original rocks are listed in Table 1.

The geometric ratio of the model is $c_l = 1:200$, and the bulk density of the model material is $c_r = 1.5\ \mathrm{t/m^3}$.

(6) Time similarity:

$$\alpha_t = \frac{t_{\mathrm{H}}}{t_{\mathrm{m}}} = \sqrt{\alpha}, \tag{6}$$

where t_{H} is the time spent on the prototype and t_{m} is the time spent on the model.

(7) Calculation of the advancement speed of the working face on the model: calculated by the time ratio formula $t_{\mathrm{H}}/t_{\mathrm{m}} = \sqrt{\alpha_L} = \sqrt{200} = 14.14$, $t_{\mathrm{m}} = t_{\mathrm{H}}/14.14$, the actual working hours on the prototype are actually 24 hours, while the actual working hours on the model are calculated on the basis of the above formula.

$$t_{\mathrm{m}} = \frac{24}{14.14} = 1.69\ \text{hours} = 102\ \text{minutes}. \tag{7}$$

The working face is pushed 2.4 m per day, which takes about 102 minutes to cut 3 footage. On the model, the working face is stoped every 17 minutes and pushed 0.2 cm with one footage. At this speed, the model is excavated until the stopping line of the working face.

2.2.2. Overall Design of Physical Similarity Model (along the Strike Profile)

(1) A physical similarity model is established. The model height includes part of the overlying strata of the 11–2# coal. The width of the model can be simultaneously satisfied so that the 11–2# coal working face can be fully mined and not affected by the mining boundary.

(2) The excavation of the working face was carried out to analyze the law of mine pressure in the direction of mining of 11–2# coal seam.

2.3. Experimental Requirements. The site location of physical similarity simulation experiment is E1108 working face of Xinji No. 2 Mine. The specific design requirements of the model experiment are as follows:

(1) The preparation of similar simulation materials is made according to the strength of rock and rock mass provided by Xinji No. 2 Mine.

Table 1: Mechanical parameters of coal and rock mass by similar materials.

No.	Lithology	Elastic modulus (GPa)	Density 10^3 (kg m^{-3})	Compressive strength (MPa)	Cohesion (MPa)	Internal friction angle (°)
1	Mudstone	10.2	1.7	41.52	1.22	39
2	Fine sandstone	35	2.6	64.09	23.1	37.5
3	Medium coarse-grained sandstone	19.2	2.4	58.52	4.5	40
4	Mudstone (containing variegated mudstone)	11.6	1.8	42.90	0.69	39
5	Fine sandstone	35	2.6	64.09	23.1	37.5
6	Mudstone	10.2	1.7	41.52	1.22	39
7	Fine sandstone	35	2.6	64.09	23.1	37.5
8	Mudstone (sandy mudstone)	11.6	1.8	42.90	0.69	39
9	Mudstone	10.2	1.7	41.52	1.22	39
10	Sandstone and mudstone	11.6	1.8	42.90	0.69	39
11	Mudstone	10.2	1.7	41.52	1.22	39
12	Sandy mudstone	11.6	1.8	42.90	0.69	39
13	Fine sandstone	35	2.6	64.09	23.1	37.5
14	Mudstone	10.2	1.7	41.52	1.22	39
15	Sandy mudstone	11.6	1.8	42.90	0.69	39
16	Fine sandstone	35	2.6	64.09	23.1	37.5
17	Mudstone	10.2	1.7	41.52	1.22	39
18	Fine sandstone	35	2.6	64.09	23.1	37.5
19	Mudstone	10.2	1.7	41.52	1.22	39
20	Fine sandstone	35	2.6	64.09	23.1	37.5
21	Mudstone	10.2	1.7	41.52	1.22	39
22	Siltstone	16	2.1	52.16	10.5	35
23	Sandy mudstone	11.6	1.8	41.52	0.69	39
24	Fine sandstone	35	2.6	64.09	23.1	37.5
25	Sandy mudstone	11.6	1.8	41.52	0.69	39
26	Fine sandstone (including mudstone)	35	2.6	64.09	23.1	37.5
27	Mudstone	10.2	1.7	41.52	1.22	39
28	Sandy mud (including mudstone)	11.6	1.8	42.90	0.69	39
29	Mudstone	10.2	1.7	41.52	1.22	39
30	Fine sandstone	35	2.6	64.09	23.1	37.5
31	Mudstone (with a small amount of fine sandstone)	11.6	1.8	41.52	0.69	39
32	Fine sandstone	35	2.6	64.09	23.1	37.5
33	Sandy mudstone	11.6	1.8	42.90	0.69	39
34	Siltstone	16	2.1	52.16	10.5	35
35	Mudstone	10.2	1.7	41.52	1.22	39
36	Fine sandstone	35	2.6	64.09	23.1	37.5
37	Mudstone	10.2	1.7	41.52	1.22	39
38	Sandy mudstone	11.6	1.8	42.90	0.69	39
39	Mudstone	10.2	1.7	41.52	1.22	39
40	Piebald mudstone	10.8	1.7	42.05	1.02	39
41	Fine-grained quartz sandstone	35	2.6	64.09	23.1	37.5
42	Sandy mudstone	11.6	1.8	42.90	0.69	39
43	Fine sandstone	35	2.6	64.09	23.1	37.5
44	Mudstone	10.2	1.7	41.52	1.22	39
45	Fine sandstone	35	2.6	64.09	23.1	37.5
46	Sandy mudstone	11.6	1.8	42.90	0.69	39
47	Mudstone	10.2	1.7	41.52	1.22	39
48	Mudstone (containing fine sandstone)	11.6	1.8	42.90	0.69	39
49	Sandy mudstone	11.6	1.8	42.90	0.69	39
50	13–1# coal seam			2.61		
51	Mudstone	10.2	1.7	41.52	1.22	39
52	Sandy mudstone	11.6	1.8	42.90	0.69	39
53	Mudstone	10.2	1.7	41.52	1.22	39
54	Piebald mudstone	10.8	1.7	42.05	1.02	39
55	Sandy mudstone	11.6	1.8	42.90	0.69	39
56	Fine sandstone	35	2.6	64.09	23.1	37.5
57	Sandy mudstone	11.6	1.8	42.90	0.69	39
58	Medium sandstone	19.2	2.4	55.86	4.5	40
59	Mudstone	10.2	1.7	41.52	1.22	39

Table 1: Continued.

No.	Lithology	Elastic modulus (GPa)	Density 10^3 (kg m^{-3})	Compressive strength (MPa)	Cohesion (MPa)	Internal friction angle (°)
60	Fine sandstone	35	2.6	51.47	23.1	37.5
61	Sandy mudstone	11.6	1.8	42.17	0.69	39
62	Fine sandstone	35	2.6	72.51	23.1	37.5
63	Mudstone	10.2	1.7	44.52	1.22	39
64	Sandy mudstone	11.6	1.8	43.62	0.69	39
65	Mudstone	10.2	1.7	45.98	1.22	39
66	Fine sandstone	35	2.6	43.71	23.1	37.5
67	Mudstone	10.2	1.7	34.06	1.22	39
68	11–2# coal seam			2.61		
69	Mudstone	10.2	1.7	23.67	1.22	39
70	Fine sandstone	35	2.6	64.09	23.1	37.5

(2) According to the occurrence of ore bodies and the scope of the experiment area to be mined, the ratio of the model is 1 : 200.

(3) The model is carried out on a plane strain model frame, and the size of the model body is $2.5 \times 0.2 \times 1.16$ m in length × width × height, and the actual height of the simulated prototype is 232 m (201.7 m in thickness above the roof of 11–2# coal seam) and 500 m in length.

(4) During the mining process, the stress and displacement around the model are relatively stable after the first mining is completed at the interval of each mining, and then, the second mining is carried out.

(5) During the mining process, after each mining, an effective stress and displacement measurement will be carried out after the surrounding stress and displacement are relatively stable.

(6) The tool used in the model excavation is a shovel. The shovel is composed of shovel cutter and long handle. The length and width of shovel cutter is 10 cm × 2 cm. The shovel is suitable in size. It can effectively control the speed of model excavation and ensure that the excavation process conforms to the actual situation.

(7) The pressure box manufacturer is self-made by the State Key Laboratory of Coal Resources and Safe Mining of China University of Mining and Technology. It meets the accuracy and range requirements. Each pressure box has passed the check process to ensure that the monitoring data are true and reliable.

2.4. Experimental Equipment and the Modeling Process. The plane stress model is adopted in the model. When the model is mined, the coal rock mass is regarded as an infinite boundary condition. The boundary conditions of the model are as follows: the stress boundary conditions are selected at the top of the model, the displacements in left and right directions are fixed, the horizontal and vertical displacements of the lower boundary are fixed, and the self-weight of the overlying strata is imposed on the upper part of the model according to the uniform load. The model height includes part of the overlying strata of the 11–2# coal. The width of the model can be simultaneously satisfied so that the 11–2# coal working face can be fully mined and not affected by the mining boundary. Therefore, the boundary conditions of the model meet the actual production requirements and have no effect on the data analysis.

According to the drilling comprehensive column diagram and coal and rock mechanics parameters of Xinji No. 2 Coal Mine, the ratio of similar simulation materials is determined. According to the coal and rock conditions, monitoring lines and distribution maps of measuring points of similar simulation experiments, as shown in Figures 1 and 2, the model is laid according to the design requirements.

According to the experimental conditions and the climate characteristics of Xuzhou, the wet model was used in this experiment. According to the similar material ratio table, the materials are weighed, mixed well, and layered in the model frame. Mica powder is added between the layers as natural bedding. The model must be dried for a period of time before being excavated, usually about 10 days. If there is a rainy day, it should be dried for at least 15 days.

During the laying process, the pressure sensors are arranged in two layers. The first layer is arranged in the floor of the coal seam, and the second layer is arranged in the fifth layer above the coal seam (as shown in Figure 1). After 10 days of drying, the displacement sensors are arranged according to the designed position. In order to observe the movement of the overlying strata in the mining process, four displacement monitoring lines are arranged in the model. The first and second measuring lines are arranged in the downhill mining section, the third measuring line is arranged in the synclinal axis, the fourth measuring line is arranged in the uphill mining section, and each monitoring line is provided with 3-4 displacement sensors (the actual arrangement of the displacement sensor is shown in Figure 2 and Table 2). After the 7th day, the test system began to be debugged. The experimental data were collected and recorded by the TS3890 static strain measuring and processing instrument, as shown in Figure 3.

When the vertical and horizontal stresses are added to the design level, the vertical stress to be compensated for this model is 0.03 MPa, and the data acquisition begins. The data are automatically collected, collected every 9 s, and the

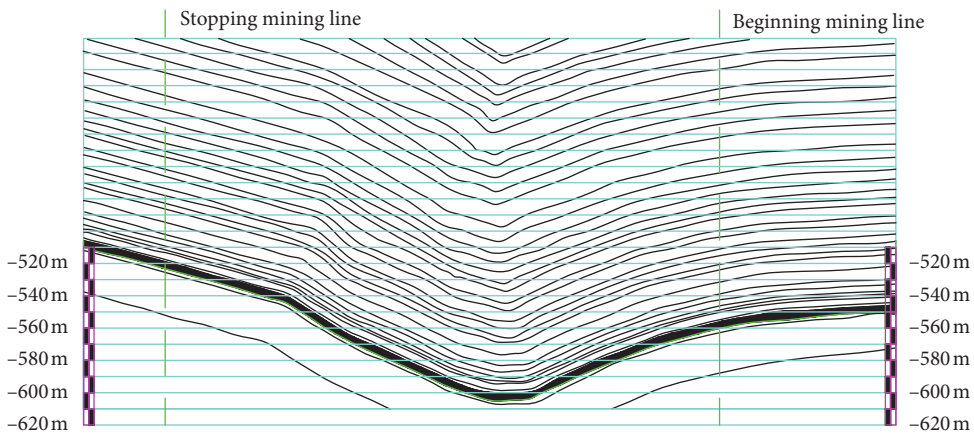

Figure 1: Distribution of coal and rock strata in physical similarity simulation experiment.

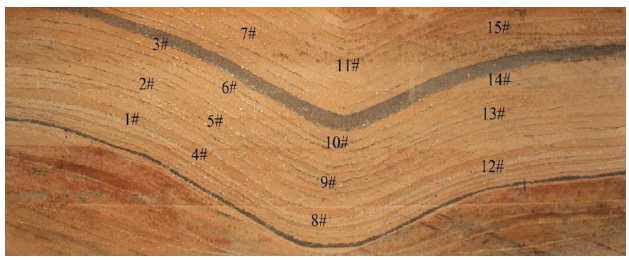

Figure 2: Layout of the displacement sensor.

Table 2: Placement of the displacement sensor.

	First measuring line				Second measuring line			
Measuring point number	1	2	3		4	5	6	7
Rock layers	Seventh	Thirteenth	Seventeenth		Seventh	Thirteenth	Seventeenth	Twenty-third
Distance from the left boundary(m)	93	105	109		181	181	189	193
Distance from the lower boundary (m)	103	129	156		73	103	121	169
	Third measuring line				Fourth measuring line			
Measuring point number	8	9	10	11	12	13	14	15
Rock layers	Seventh	Thirteenth	Seventeenth	Twenty-third	Seventh	Thirteenth	Seventeenth	Twenty-third
Distance from the left boundary (m)	263	263	255	193	379	379	375	375
Distance from the lower boundary (m)	31	65	89	139	73	109	125	173

Figure 3: TS3890 static strain measuring and processing instrument.

collected data are compared with the previously collected data. Finally, when the collected data are stable, it is used as the initial reading and stored in the disk. Excavation is then started according to the design requirements, and the data are continuously collected during the excavation process until the end of the experiment. Since the displacement sensor is mounted on the surface of the model, and some of them are mounted on the part to be excavated, these sensors move during excavation but do not affect the experimental results and their analysis.

3. Experimental Results and Analysis

3.1. Activity Lows of Rock Strata during Mining

3.1.1. Activity Lows of Rock Strata during Mining of the Downhill Mining Section. A 2.5 cm (corresponding to 5 m of the prototype; hereinafter referred to the prototype values)

open-off cut was excavated at a distance of 25 cm from the left boundary of the model. With the advancement of the working face, the hanging area of the immediate roof gradually increased. As the working face was advanced by 12.5 m, the bed separation of immediate roof strata started and vertical microfractures occurred. When the working face was cumulatively advanced by 20 m, the immediate roof reached its limit span and started the initial caving, but the hanging immediate roof did not cave completely. Complete caving of the immediate roof was observed after the cumulative advancement of the working face reached 22 m (Figure 4).

When the working face was advanced by ~46.5 m ahead of the open-off cut, the bed separation and bending subsidence of the main roof were intensified. A relatively distinct separation and bending subsidence zone was located in the left-of-center of the hanging part of the main roof. As observed in the experiment, the caving rocks of the immediate roof had formed effective support for the main roof. The initial weighting of the main roof was determined, with an interval of 46.5 m.

When the working face was advanced by 70.9 m ahead of the open-off cut, the fourth caving occurred in the immediate roof strata, with an interval of 17.4 m (intervals of the second and third caving were 16.7 and 14.8 m, respectively). Above the coal seam, the bed separation was intensified in the 2nd layer, while slight separation occurred in the 3rd and 4th layer. The 2nd, 3rd, and 4th layers showed a consistent tendency of separation and subsidence. These three layers represented the main roof in the design (Figure 5).

When regular periodic caving occurred in the immediate roof strata, there were also dramatic changes in the main roof and overlying strata. When advanced by 93.4 m ahead of the open-off cut, the working face entered an area in the angle of depression of at least 30° from that within 17°. When the working face was advanced by 132 m ahead of the open-off cut, the bed separation in the 5th layer above the coal seam was generally consistent with that observed in the main roof (i.e., 2nd to 4th layers), while the 8th and 9th layers showed slight separation. The 6th and 7th layers exhibited a consistent trend of deformation, belonging to combined deformation. The separation interval between the 7th and 8th layer was ~200 mm; the separation interval between the 5th and 6th layer was ~600 mm; and the separation interval between the 4th and 5th layer was ~700 mm. The 2nd to 4th layer (i.e., main roof) belonged to combined deformation. Additionally, vertical fractures appeared at the leftmost side of the 2nd and 3rd layers in the roof above the goaf (above the open-off cut).

When the working face was advanced by 140 m, a large area of breakage appeared at the left end of the 2nd and 3rd layers, with periodic weighting of the main roof and a caving length of 28 m. At this point, the separation interval between the 4th and 5th layer reached 1900 mm (Figure 6).

Generally, the downhill mining section could be subdivided into two sections according to the angle of depression. The front section had a smaller angle of depression (with an average of ~17°) and a length of ~86.8 m, while the rear section had a larger angle of depression (with an average of ~35°) and a length of ~117 m. After the main roof caved thoroughly in the front section, the most prominent bed separation was observed in the upper part of the rear section 50 m from the coal wall; the separation interval between the 3rd and 4th layer had expanded to ~600 mm, the separation intervals between the 6th and 7th layer reached ~400 mm, and the separation of the 8th layer was aggravated. In the front section, the bed separation between the 5th and 6th layer was obviously closed. At this point, bed separation in the front section had developed upwards to the 10th layer above the coal seam.

When the cumulative advancement of the working face reached 146 m, the main roof strata partially presented rotary instability, with a large area of breakage. The length of the breakage was ~30 m, and the breaking strata were consistent with the 2nd and 3rd layers. A three-hinged arch balance was formed after breakage: the rear caving section was supported by the goaf, while the front section was hinged with rock strata above the coal wall. Additionally, there was considerably increased strata separation above the 3rd layer. According to on-site measurements, the separation interval was ~2100 mm between the 3rd and 4th layer, while it was ~1000 mm between the 5th and 6th layer. The bed separation of the 10th and 11th layers had expanded from the front section to ~50 m away from the coal wall (Figure 7).

When the dip angle of downhill mining was increased for the working face, the caving rocks at the goaf side slipped toward the coal wall side. These rocks played a partial role in supporting the immediate roof. Moreover, during downhill mining, the vertical fractures in the immediate roof tended to be compressed and closed due to the self-weight of the strata. All these factors delayed immediate roof caving while extending the caving interval. When the working face was advanced by 175.2 m ahead of the open-off cut, the immediate roof caved with an interval of 13.6 m. Meanwhile, in the front section, the bed separation of the 8th to 13th layer was closed, with gradual compression of strata below the 8th layer. In the rear section, two or three obvious vertical fractures occurred in the coal wall at the right side of the 2nd and 3rd layers in the roof. Between the previous caving and the current caving, the overlying strata (from the 2nd layer through the 18th layer to the 22nd layer) showed a marked overall subsidence in the rear section.

When the working face was cumulatively advanced by 189 m, the immediate roof caved with an interval of 14 m. The migration trends of the main roof (2nd and 3rd layers) and the immediate roof were relatively consistent. As the immediate roof caved, the main roof lost its support and showed obvious pseudoplastic bending deformation due to the effects of self-weight and overlying strata. There was marked bending subsidence in strata overlying the main roof until the 18th layer of rock (coal) strata. The overlying layers of rock strata were damaged by various fractures and appeared in a mutually extruded state, which formed a beam-like balance and showed obvious pseudoplastic bending subsidence due to the effects of self-weight and overlying strata.

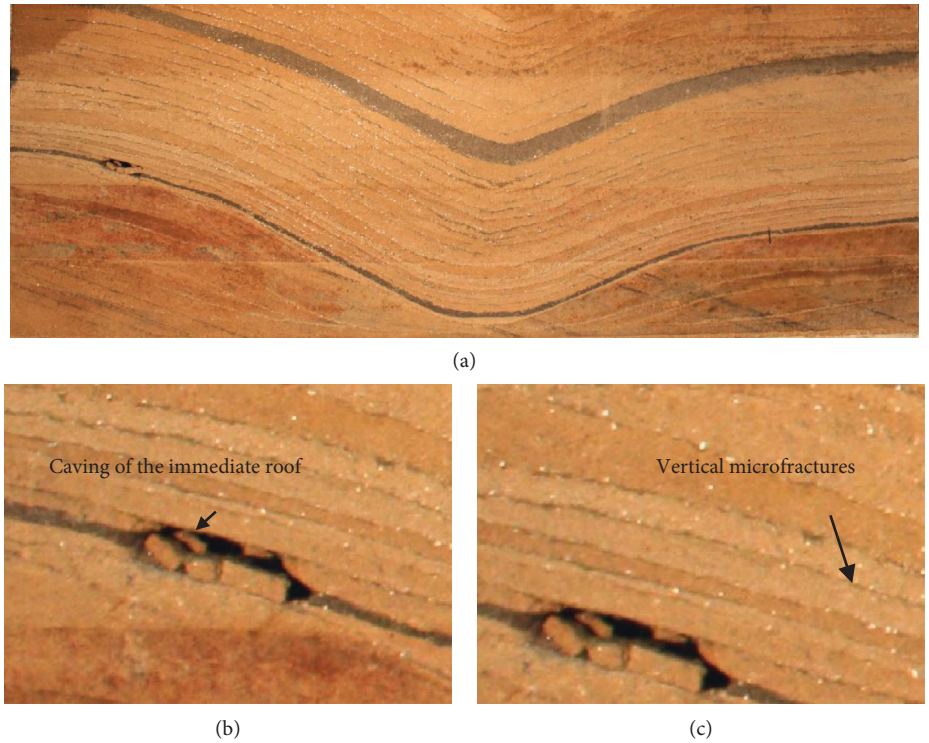

Figure 4: First caving of the immediate roof. (a) State before the roof collapses. (b) Caving of the immediate roof. (c) Vertical microfractures development.

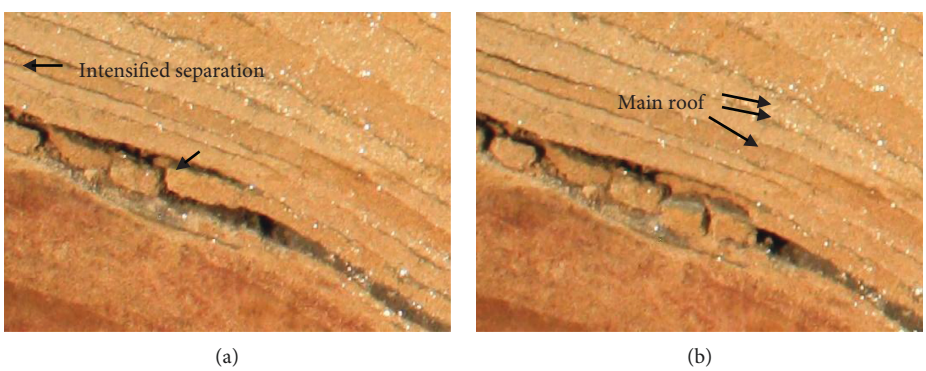

Figure 5: Activity of overlying strata. (a) Separate fractures. (b) The position of the main roof.

3.1.2. Activity Lows of Rock Strata during Mining of the Synclinal Axis (Bottom of the Pan). When it was advanced to the vicinity of the synclinal axis (bottom of the pan), the working face showed a major change in the angle of depression. As the working face was cumulatively advanced by 208 m, immediate roof caved, with a cantilever length of ~16 m before caving. Vertical fractures occurred in the 2nd to 6th layer and gradually expanded to ~300 mm with mining. Different layers showed a consistent trend of movement compared with the front section. Fractures had been fully developed inside the main roof and its overlying strata, which were overall deformed with the immediate roof deformation. Currently, the most obvious fracture development and bed separation appeared in an area between 20 and 70 m from the coal wall. Within this area, the bed separation was extended to a highest level of the 14th layer.

When the working face was advanced by 250 m, there was periodic weighting of the main roof with an interval of ~23 m. Partial strata of the main roof overall caved, and the caving site was in a place where vertical fractures were fully developed. The overlying strata overall subsided after the main roof caved. After caving, vertical fractures appeared at a distance of ~10 m from the coal wall in the 2nd to 8th layer, leading to the formation of a new potential caving area between 10 and 22 m from the coal wall in the 4th to 6th layer. Slight fractures also occurred in the 13th–15th layer and the 18th–21st layer at the corresponding locations. After the main roof caved completely, vertical fractures generally being connected in the vertical and horizontal directions were formed in the 2nd to 20th layer of the overlying strata at the bottom of the pan. This indicated that the overlying strata suffered dramatic disturbance in the synclinal axis (Figure 8).

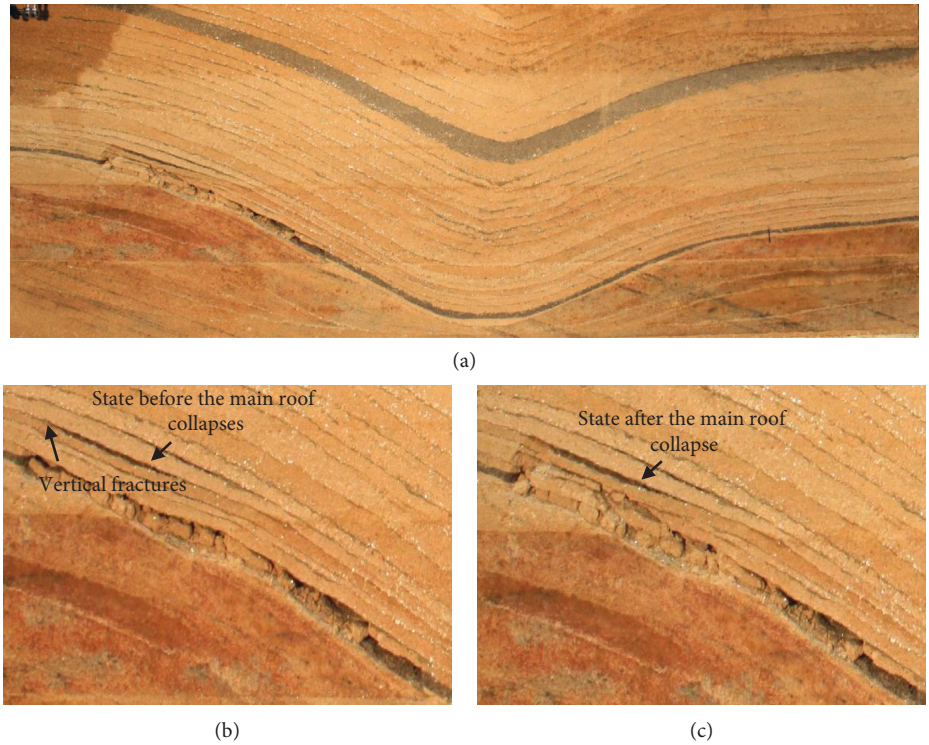

Figure 6: Periodic pressure of the main roof. (a) State after the main roof collapses. (b) Fissures and separation development. (c) The scope of the main roof collapses.

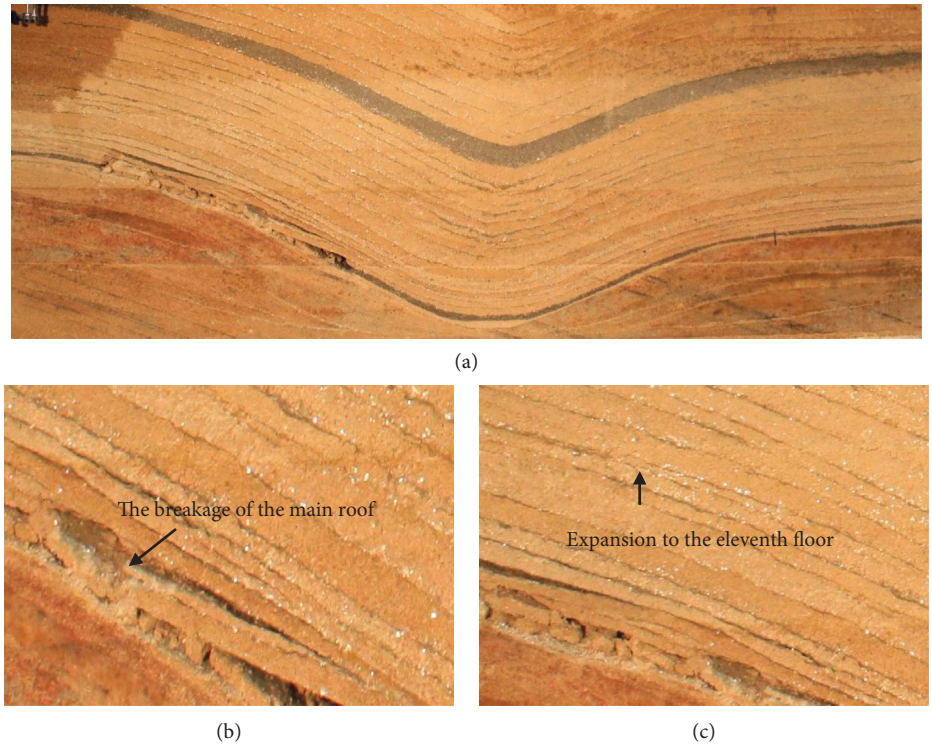

Figure 7: Periodic pressure of the main roof. (a) The whole picture of the model after the breakage of the main roof. (b) The breakage of the main roof. (c) Separation of the overlying strata.

Near the synclinal axis (bottom of the pan), the immediate roof and the main roof exhibited distinctly different lows of breakage caving compared with the downhill mining section. Specifically, the caving cycle of the main roof was considerably shortened (one time of main roof weighting for every one to two times of immediate roof caving), and the intensity of main roof caving and weighting was markedly increased; along with the main roof weighting, the overlying strata also showed remarkable overall bending subsidence, while the bed separation of overlying strata was weakened.

3.1.3. Activity Lows of Rock Strata during Mining of the Upward Mining Section. When the working face was cumulatively advanced by 267 m, the upward mining stage started. Vertical fractures perpendicular to the coal seam were formed in the 2nd to 8th layer and connected the vertical fractures at the bottom of the pan in the 8th layer. When the working face was cumulatively advanced by 285 m, the strata overlying the working face were deformed, forming three distinct vertical fractures that were completely or partially connected. The first fracture ranged from the 5th to 21st layer, the second spanned from the 5th to 14th layer, and the third was within the range of the 5th to 18th layer. These generally developed, and connected vertical fractures could clearly reflect the overall deformation of overlying strata in different areas.

When the working face was advanced by 306 m, the main roof of the working face (with a caving interval of 21 m) showed overall bending subsidence caving in an inverted step shape shortly after the immediate roof caved. Owing to the support of the 5th layer, there was little deformation in the layers above the main roof, and the bed separation between the 4th and 5th layer reached a height of 600 mm. Slight vertical fractures occurred above the coal wall in the main roof (2nd to 4th layers) of the overlying strata in the goaf, while no obvious bed separation was observed above the 4th layer (Figure 9).

When the working face was advanced into the upward mining section, the destruction of main roof was not as drastic as that in the axis. The previous breakage caving appeared as overall bending subsidence. Meanwhile, the overlying strata also rapidly subsided as a whole, resulting in little development or fast closure of bed separation between strata. The cantilever of the immediate roof in the mining section was subjected to a component force toward the synclinal axis, and the immediate roof (above the coal wall) was prone to form vertical fractures with a relatively short caving interval; it generally caved along with mining. Meanwhile, the activities of overlying strata were markedly affected by mining, and vertical fractures were developed in the strata. This was especially evident in the 18th to 27th layer, but not obvious in the 2nd to 17th layer (Figure 10).

When the working face was advanced by 443 m ahead of the open-off cut, the mining ended and the working face had a moderate angle of elevation near the stop line. The cantilever beam of the immediate roof was ~7 m long at the end of the mining. Meanwhile, the bed separation of the overlying strata became relatively obvious again. The bed separation between the 2nd and 3rd layer reached a height of 1400 mm, while the bed separation between the 4th and 5th layer was also 1400 mm. Slight separation also occurred through the 5th to 18th layers (Figure 11).

Based on the above phenomena and analyzes, the activities of overlying strata had the following characteristics during mining of the working face:

(1) The immediate roof in the downhill mining section generated a component force toward the coal wall along the bedding plane, which resulted in a trend of closing fractures in the roof. Additionally, it was supported by falling rocks in the goaf and thus was unlikely to cave, with a relatively large caving interval (m). However, in the downhill mining section, the gangue in the goaf tended to enter the workspace, which required proper implementation of protective measures. In the synclinal axis area, the characteristics of immediate roof caving were similar to those observed in the downhill mining section. In the upward mining section, the roof was subjected to a component force toward the synclinal axis. The roof was affected by a pulling force, and vertical fractures were easily formed at the root of the cantilever beam of the immediate roof (above the coal wall), which had a relatively short caving interval (m) and generally caved along with mining. This indicated that it was difficult to control the roof in the upward mining section.

(2) Across different sections, the main roof and its overlying strata showed varying characteristics of breakage caving. During upward mining, the main roof was unlikely to cave, with a relatively long caving interval; each layer of the overlying strata successively shifted from an undisturbed state into a disturbed state. The activities of the strata were mostly shown in the form of bed separation. As the working face was advanced, the separation area was gradually developed upwards. In the synclinal axis, the caving cycle of the main roof was considerably shortened (one time of the main roof weighting for every one to two times of immediate roof caving), while the intensity of the main roof caving and weighting was markedly increased. Along with main roof weighting, different layers of the overlying strata also showed obvious overall bending subsidence. Meanwhile, the bed separation of overlying strata was weakened. In the upward mining section, the main roof had no obvious breakage caving and generally presented bending subsidence caving as the immediate roof caved; the subsidence and separation of overlying strata were not as obvious as observed during the other stages.

(3) The bed separation of overlying strata was most distinct in the downhill mining section and the synclinal axis area. It was observed that the distinct area of bed separation was extended to a highest of the 14th layer. Within this area, bed separation gradually expanded forward as the working face was

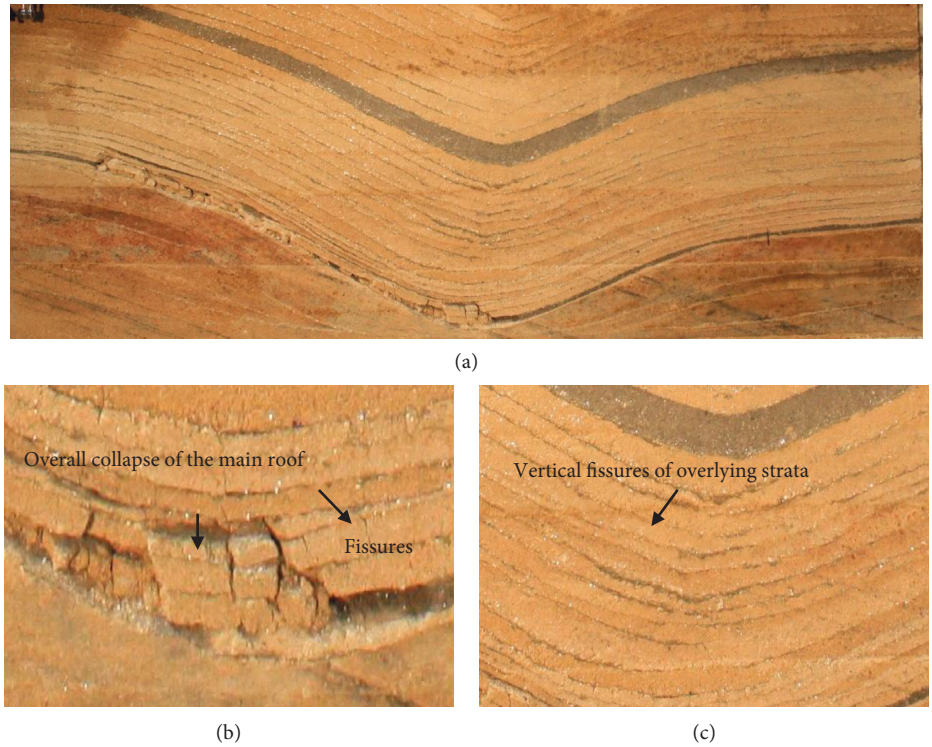

Figure 8: The main roof collapses in the synclinal axis and fissure development of the overlying strata. (a) The whole picture of the model after the breakage caving of the main roof. (b) Overall collapse of the main roof. (c) Vertical fissures of the overlying strata.

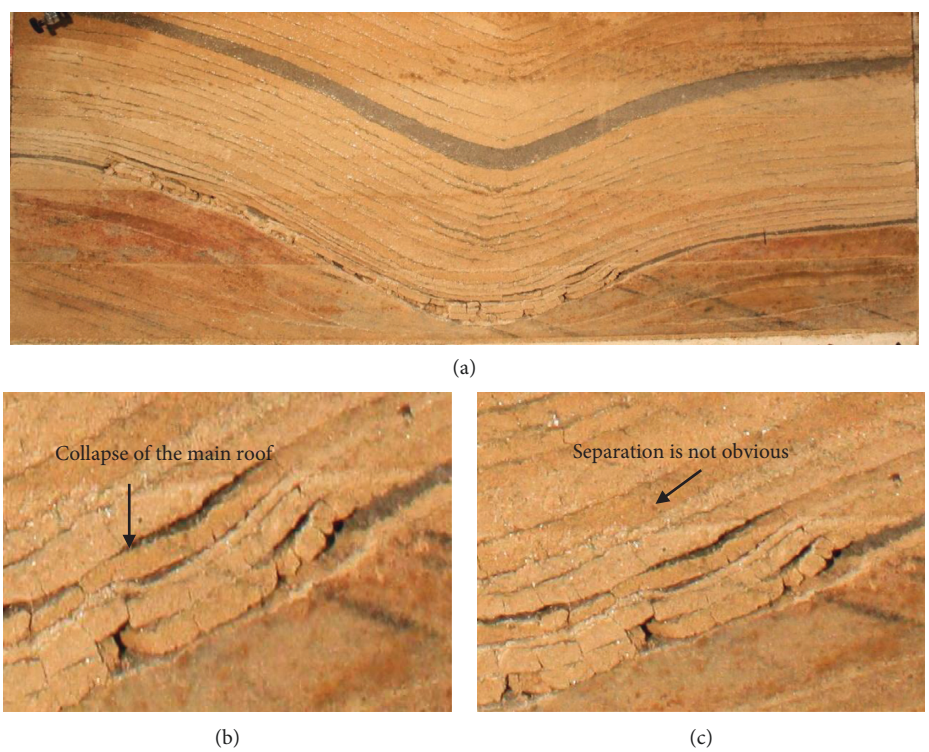

Figure 9: Periodic pressure of the main roof in the downhill mining section. (a) The whole picture of the model after the breakage caving of the main roof. (b) Collapse of the main roof. (c) The state of the overlying strata.

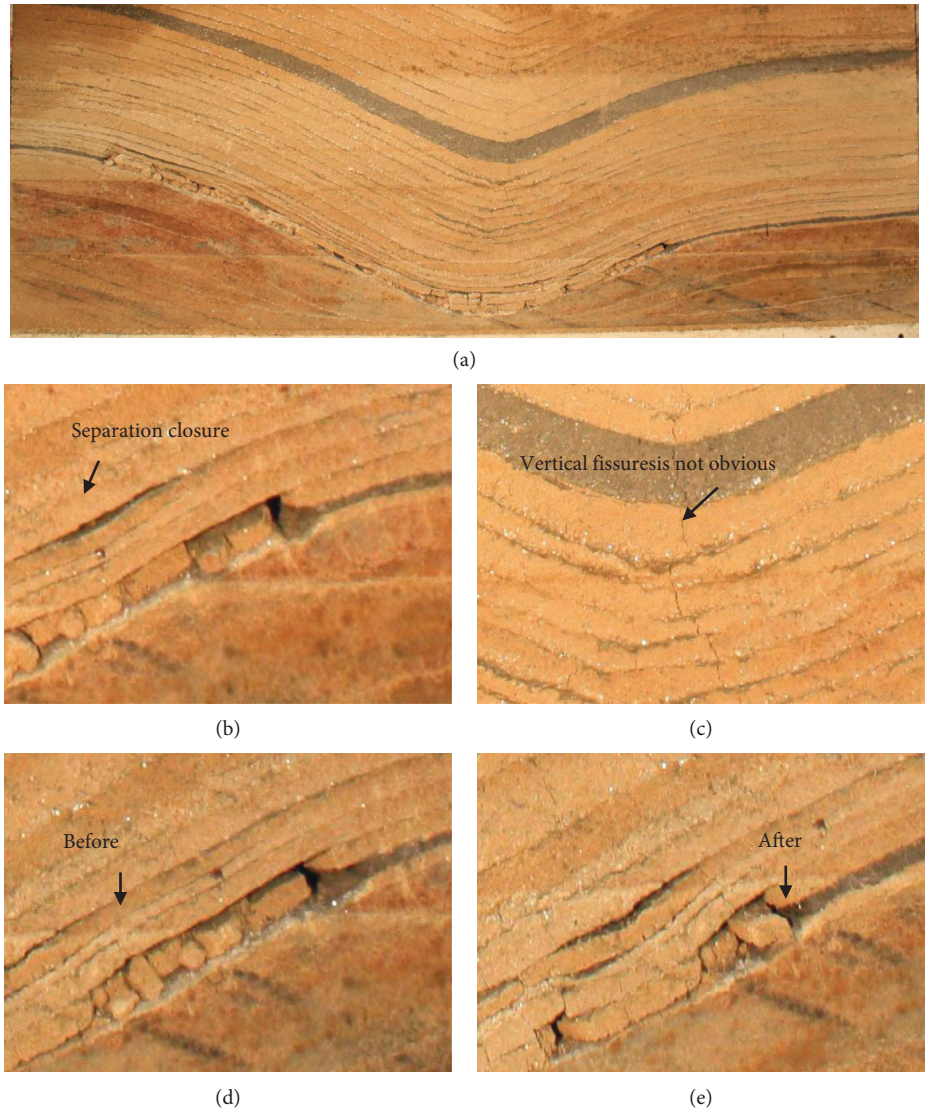

Figure 10: Periodic pressure of the main roof in the downhill mining section. (a) The whole picture of the mode. (b) Separation closure. (c) Vertical fissures of the overlying strata. (d) Before the bending caving of the main roof. (e) After the bending caving of the main roof.

advanced. When the working face was advanced into a certain range, the separation fractures formed during the earlier mining stages were gradually closed from top to bottom.

(4) Based on the observation after complete mining of the working face, obvious vertical fractures were developed in multiple areas. Multiple vertical fractures were formed in the 2nd to 17th layer above the open-off cut, with a maximum height of ~70 m from the working face. Additionally, three obvious vertical fractures connected completely or partially were formed in the overlying strata in the synclinal axis, and the vertical fractures in this area were mostly developed from top to bottom based on field observation. Due to the vertical fractures in these two areas, the overlying strata had been overall damaged from the open-off cut to the synclinal axis. Within this range, the rock mass tended to slip toward the axis along the coal seam strike, exerting an extrusion effect on the roof in the synclinal axis. The distribution of the vertical fractures is shown in Figure 12.

3.2. Influence of Overlying Strata Movement on Water Prevention and Control. The movement and destruction of overlying strata have obvious zonality. From the goaf to the surface, the failure scope of overlying strata is gradually enlarged and the degree of failure is gradually weakened. The movement and destruction of overlying strata from bottom to top are caving zone, fracture zone, and bending subsidence zone, respectively.

The caving zone refers to the rock strata which lose continuity and fall to the goaf with irregular or layered rock blocks. There are many gaps and strong connectivity between the rock strata. The caving zone is the passage for water and sediment to break into the underground well. It is

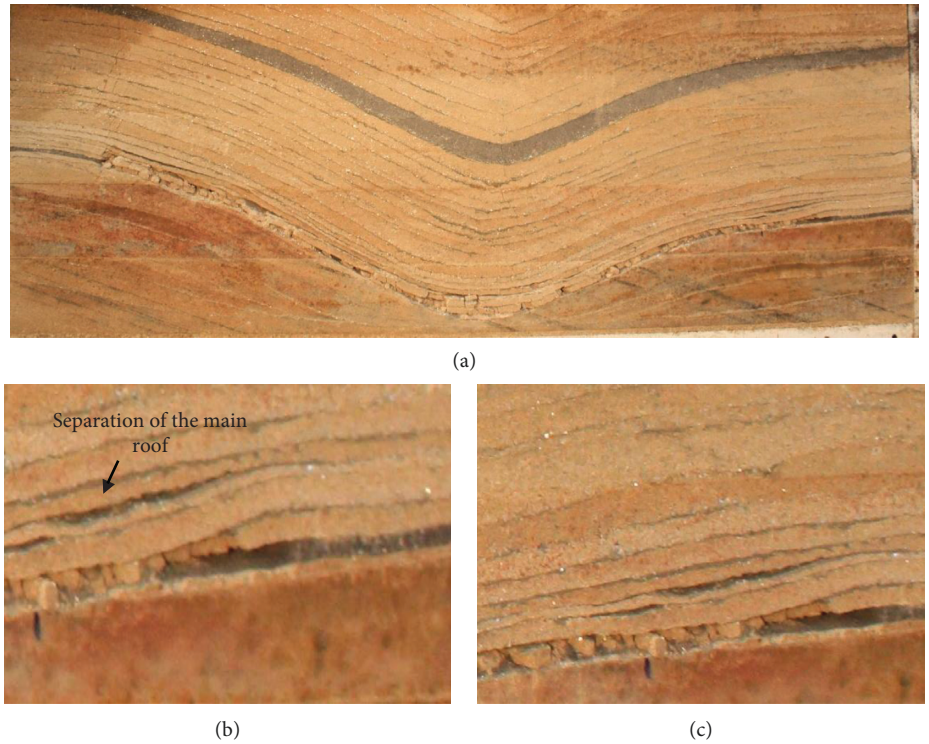

Figure 11: Activity characteristics of the overlying strata at the end of mining. (a) The whole picture of the mode after mining. (b) Separation of the main roof. (c) Separation of overlying strata.

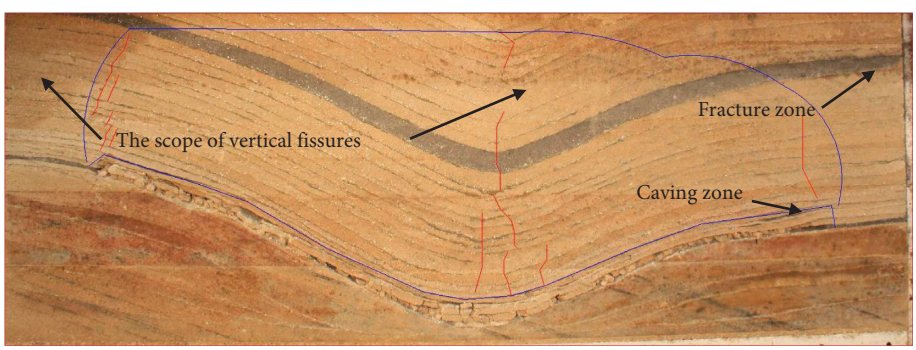

Figure 12: The scope of caving zone, fracture zone, and vertical fissures.

also the place where the gas escapes and accumulates. In this simulation experiment, the immediate roof and the majority of the main roof constitute the caving zone, as shown in Figure 12.

The fracture zone is located above the caving zone and has a water-conducting fracture that is connected with the goaf. It can be divided into two types: one is vertical or oblique new-born tension fracture, which is mainly caused by downward bending and tension of rock layers. It can pass through the rock layers partly or completely, but the rock mass on both sides can basically maintain the continuity of layers; the other is separated fracture along the layers. This fissure is mainly caused by the large difference in mechanical properties of the rock layers and the downward movement of the rock layer asynchronously. The total amount of surface subsidence is less than the thickness of the coal seam. In addition to the fragmental expansion factor of caving rock, the separation of the fracture zone is also the main reason. The fracture zone develops upwards as the mining area expands. When the mining area expands to a certain extent, the fracture zone height reaches the maximum. At this time, the mining area continues to expand, the height of the fracture zone basically no longer develops, and the rock strata movement tends to be stable over time. The vertical and separate fractures of the fracture zone gradually close from the top to the bottom.

The vertical fracture is the water conduction channel of the upper and lower strata, and the separated fracture is the channel of water storage and water conduction in the same rock layer. There may also be separation cracks above the fracture zone, which can indirectly guide water and accumulate water, but because the vertical fracture is not

developed, it cannot communicate with the fracture zone. If the fractured zone affects the water body, the separated layer fracture and the vertical fracture are connected, and the water conductivity is obviously increased, and the water can be introduced into the goaf under the shaft. Therefore, it is of great significance to find out the scope of the water-conducting fracture zone for the prevention and control of water in the working face.

In the process of model mining, the phenomenon of layer separation is more serious, especially in the downhill mining section and the synclinal axis area, and the obvious layer separation can be seen by naked eyes and extended to the 14th layer. The vertical fissures are well developed in many areas: several vertical fissures are developed in the second to seventeenth layers above the open-off cut, and the highest point is about 80m away from the working face; three distinct vertical fissures are formed in all or part of the overlying strata on the synclinal axis, the first from the fifth layer to the twenty-seventh layer, the second from the fifth layer to the fourteenth layer, and the third from the fifth layer to the eighth layer; the highest point is about 160m; the vertical fracture development is more obvious in the uphill mining section, so the scope of the fracture zone can be determined, as shown in Figure 12.

According to the hydrogeological data, the overburden aquifer on the E1108 working face is mainly composed of the Cenozoic loose aquifer, the nappe gneiss fracture aquifer, and the nappe Cambrian limestone aquifer.

(1) The Cenozoic loose aquifer is rich in water. It is more than 270 m away from the working face and is more than 100 m above the peak of the fracture zone, separated by gneiss in the middle. Therefore, this layer of water has no direct influence on the mining of the working face.

(2) The nappe gneiss fissure aquifer has uneven water richness and weak water richness. The lower part of the nappe is contacted with the clip stratum by the Fufeng thrust fault. Through the fault fissure, the fracture water of the gneiss has certain recharge to the clip aquifer. The working surface is about 120–277 m away from the gneiss stratum. Therefore, gneiss fissure water during mining may introduce water into the working face through water-conducting fissures. Therefore, a targeted water control scheme should be specified.

(3) The nappe Cambrian limestone aquifer, which is mainly dominated by limestone, has uneven water richness, and the shallow part is subjected to weathering, the rock mass is in a loose structure, and the water richness is relatively strong; below and deep fractures are not developed, and the water richness is relatively small. The roof of E1108 working face is directly covered by the Cambrian strata, and the water in this aquifer is likely to be introduced into the working face through separation fissures or vertical guide water fissures, which will cause great safety hazards to the mining face.

3.3. Abutment Pressure Changes in Roof and Floor Strata with Advancement of Working Face. To analyze the changes of abutment pressure distribution in the roof at different locations of the working face with the advancement of working face, we selected pressure cells from the roof strata as the subjects for the analysis of abutment pressure in the roof, including pressure cells 13 and 15 in the downhill mining section, pressure cell 17 in the synclinal axis, and pressure cells 18 and 19 in the upward mining section. Additionally, we selected pressure cells 3, 5, 7, 8, and 9 from the corresponding locations in the floor as the subjects to analyze the abutment pressure in the floor. The curves of abutment pressure changes at different locations of the roof and floor strata were drawn (Figures 13–17), and the changes of abutment pressure throughout the mining process were analyzed at each location in the roof and floor. Additionally, the distribution lows of abutment pressure were summarized during downhill and upward mining of the working face. The abscissa indicates the distance between the measuring point and the coal wall of working face, with the working face advanced from left to right; the zero point is defined as the location when the working face was advanced to right below (above) the pressure cell.

As shown in Figure 13, at pressure cell 13, the abutment pressure of the roof went through a stress increase zone and a stress decrease zone; subsequently, it entered a stress increase zone again after the working face was advanced by ~170 m. During mining, the pressure peak occurred when the working face was advanced by ~10 m; thereafter, the pressure rapidly decreased due to roof weighting and caving, with a minimum value that was lower than the in situ rock stress by ~750. After the working face was advanced by ~160 m, the decrease zone was affected by compaction of strata in the goaf and pressure transfer of strata in the front section (a component force toward the coal wall along the bedding plane of breaking strata in the front section); thus, the abutment pressure entered an increase zone and reached a maximum of ~400. Pressure cell 13 was set in a transition zone between the front and rear sections of the downhill mining stage. As shown in the figure, this site and the coal wall at the left of the open-off cut jointly played a role in supporting the front section as a beam with hinged-hinged ends. This structure was able to bear the component force of rightward slip from the damaged overlying strata in the front section, leading to a considerable increase in the pressure. There was also a peak of abutment pressure during the mining of working face, but the absolute value was small, with a maximum of 20.

Pressure cell 15 was located in the middle part of the rear section in the downhill mining stage, ~150 m ahead of the open-off cut. The abutment pressure at this site peaked after the working face was advanced by ~15 m. Subsequently, breakage caving occurred in the overlying strata, and the embedded site of the pressure cell in the roof was unloaded, resulting in a rapid decrease in the abutment pressure. There was generally no change in the abutment pressure of the floor, indicating that the mining process caused little disturbance to the floor.

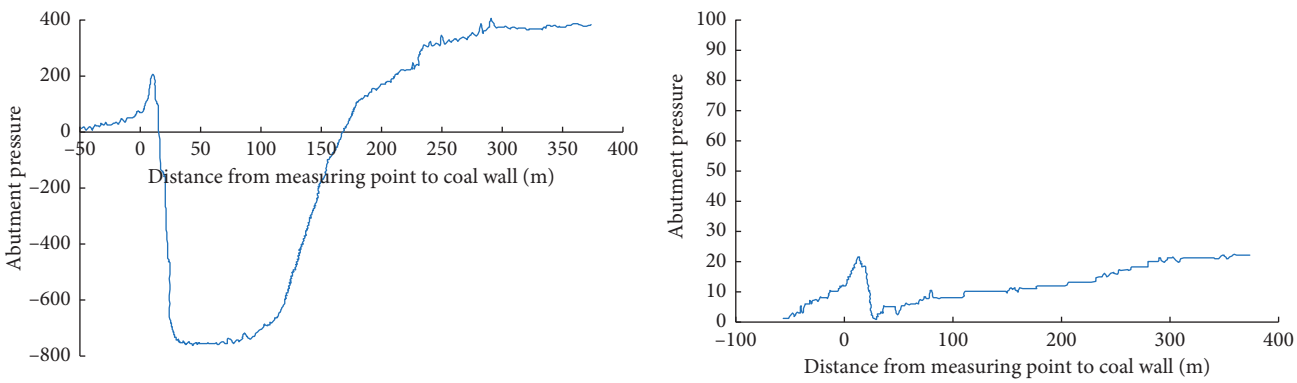

(a) (b)

Figure 13: The changing curve of the abutment pressure in the roof as the advancement of working face at the floor strata 17 m away from the open cut (in the downhill mining section). (a) Roof (located at pressure cell 13). (b) Floor (located at pressure cell 3).

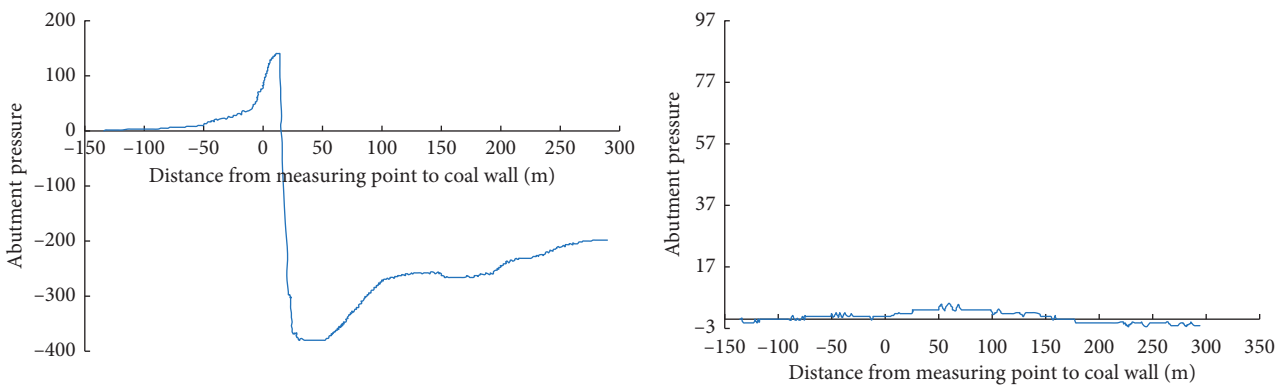

(a) (b)

Figure 14: The changing curve of the abutment pressure in the roof as the advancement of working face at the floor strata 150 m away from the open cut (in the downhill mining section). (a) Roof (located at pressure cell 15). (b) Floor (located at pressure cell 5).

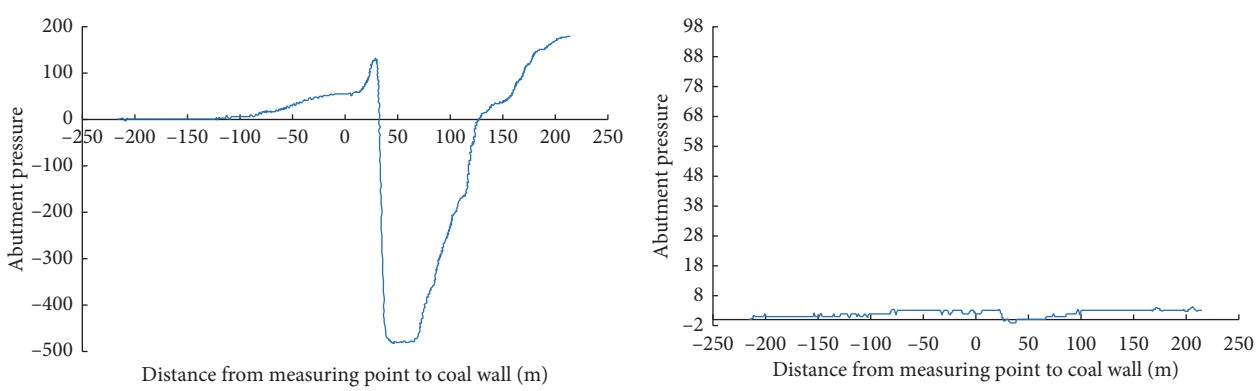

(a) (b)

Figure 15: The changing curve of the abutment pressure in the roof as the advancement of working face at the floor strata 240 m away from the open cut (in the synclinal axis). (a) Roof (located at pressure cell 17). (b) Floor (located at pressure cell 7).

Pressure cell 17 was located at the bottom of the pan (synclinal axis), ~250 m ahead of the open-off cut. Similar to the result for pressure cell 13, pressure cell 17 at this site also went through three stages and there was an increase zone of abutment pressure in the goaf after a decrease zone. Based on the observation of overlying strata movement at this site during simulation, there was relatively intense roof breakage in the synclinal axis. The caving cycle of the main roof was considerably shortened (one time of main roof weighting for every one to two times of immediate roof caving), while the

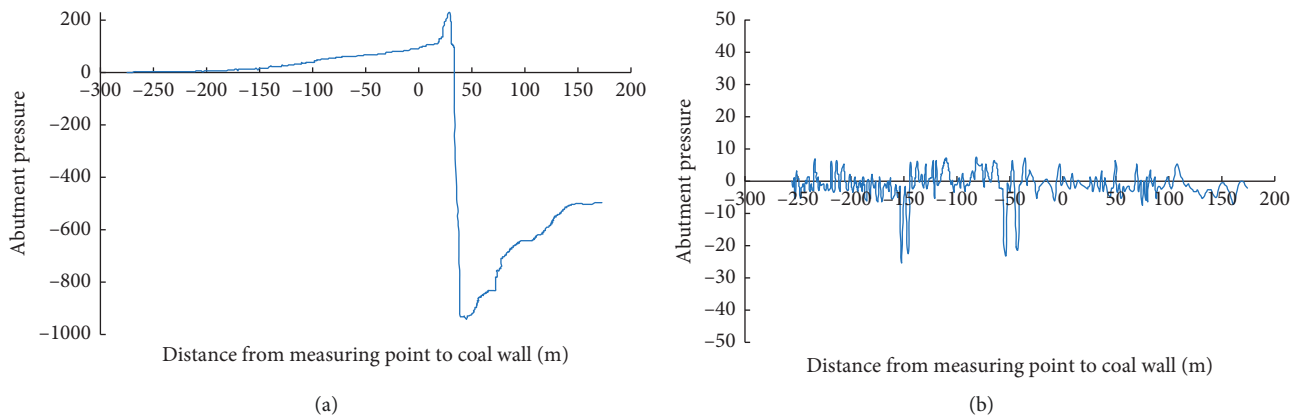

Figure 16: The changing curve of the abutment pressure in the roof as the advancement of working face at the floor strata 285 m away from the open cut (in the uphill mining section). (a) Roof (located at pressure cell 18). (b) Floor (located at pressure cell 8).

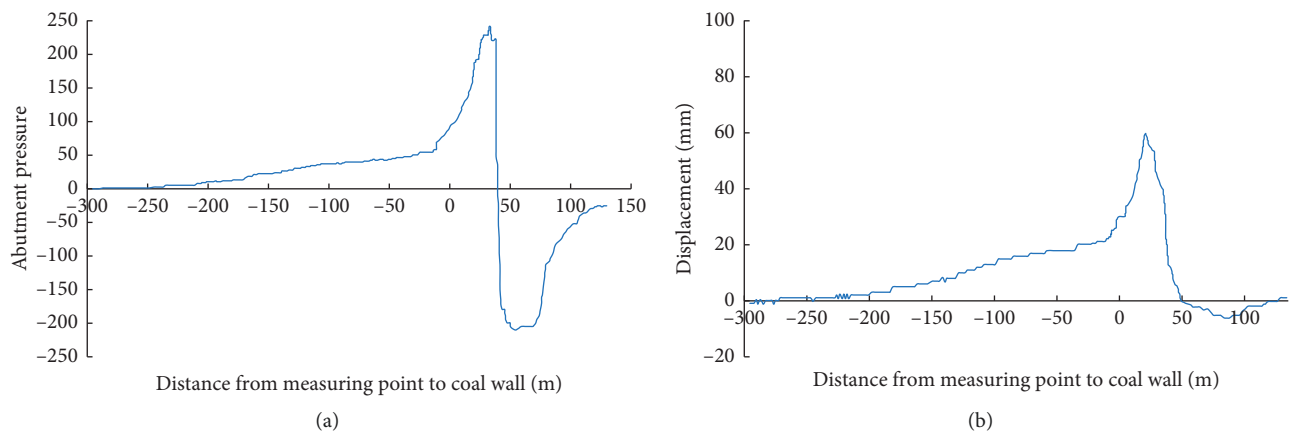

Figure 17: The changing curve of the abutment pressure in the roof as the advancement of working face at the floor strata 330 m away from the open cut (in the uphill mining section). (a) Roof (located at pressure cell 19). (b) Floor (located at pressure cell 9).

weighting intensity during main roof caving also increased markedly. Along with the breakage caving of the main roof, even the overlying strata at the uppermost part of the model showed significant overall bending subsidence and vertical fractures that were connected occurred between different layers. These phenomena indicated that the internal overlying strata had been severely damaged, while the strata at both sides tended to be extruded toward the center. Consequently, the roof at this site was subjected to not only the pressure of overlying strata but also the slip component of damaged strata at both sides toward this site simultaneously, which resulted in a considerable increase in the abutment pressure. The abutment pressure in the floor did not change markedly.

Both pressure cells 18 and 19 were located in the upward mining section. The advance abutment pressure and the abutment pressure peak in this section were markedly higher than those in the other parts before mining. After mining of the working face, a portion of the pressure from the overlying strata was transferred to the synclinal axis due to the angle of elevation of the strata. Thus, the rear abutment pressure in the goaf at the corresponding location was not as large as that in the axis. In the upward mining section, the abutment pressure in the floor changed more obviously compared with the other locations. In particular, a marked elevation of abutment pressure was observed during mining by pressure cell 9, and the peak value was close to 60, which was markedly higher than the results of the other sites.

Based on the above analysis, the distribution of abutment pressure at different positions of the working face has the following characteristics:

(1) Advanced abutment pressure: the synclinal axis is larger than the mining downhill and uphill mining sections (about 50), and the uphill mining section (90 or more) is larger than the downhill mining section (about 70); the influence range of the advance abutment pressure: the maximum of the uphill mining section is over 200 m, the synclinal axis is about 90 m, and the maximum of the downhill section is not over 60 m.

(2) The peak value of the abutment pressure appears after the mining and appears 30 m away from the measuring point of the working face in both the synclinal axis and the uphill mining section. However, the peak value of the abutment pressure appears

less than 15 m away from the measuring point of the working face in the downhill mining section. The peak value of the abutment pressure in the uphill mining section (more than 240) is larger than that in other sections (all under 140 except No. 13).

(3) The increase of the abutment pressure of the goaf occurs at the transition between the front and rear sections of the downhill mining section and the synclinal axis. The reason for the increase of the abutment pressure at the transition between the front and rear sections of the downhill mining section is that it is located at the back arch foot of the pressure arch in the front section (the front arch foot is the coal wall of open-off cut), bearing the stress component from the concentrated stress along the strike of the rock stratum in the front section. In the syncline axis, because the overlying strata on both sides slip and squeeze toward the axis after being broken by mining, the stress components along the strike of the strata on both sides are concentrated here so that the abutment pressure of the goaf increases.

(4) The variation of the abutment pressure on the floor is mostly not obvious, and the peak value is generally below 30, and the change is obvious at the pressure cell No. 9.

3.4. Analysis of Displacement Variation of Overlying Strata. In order to analyze the displacement changes of the overlying strata in different positions of the working face with the advancing process of the working face, the displacement variation curve of each measuring line is drawn to observe the subsidence characteristics of strata at different measuring points of each measuring line during the advancing process of the working face, and the movement law of the overlying strata in the mining face is summarized. The abscissa indicates the distance between the measuring point and the coal wall of the working face. The working face advances from left to right, and the zero point is defined as the position when the working face advances directly below the observation line.

From Figures 18–21, it can be seen that the displacement of the overlying strata at different positions of the working face has the following characteristics as the working face advances:

(1) In the same observation line, the displacements observed from the measurement points from the seventh layer to the twenty-third the rock layer above the coal seam are basically the same, indicating that there is an overall sinking phenomenon in the overlying layers.

There are two possibilities for the problem of the displacement curve in which the displacement of the upper layer is sometimes greater than that of the lower layer. One is the systematic error of the experiment. Since the displacement sensors are mounted on the surface of the model and part of the sensors are mounted on the site to be excavated, these sensors are moving in the excavation process. However, the actual maximum subsidence of the rock layer in the model is only about 1 cm, it is inevitable that a 1 mm error is generated; the second possibility is that the displacement of the upper

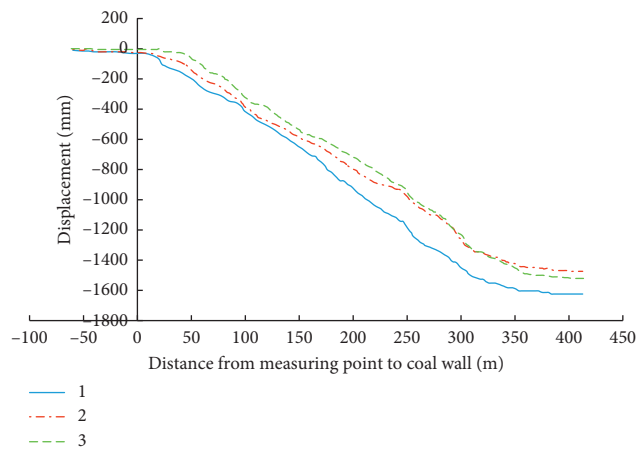

Figure 18: The displacement curves of the overlying strata at the first measuring line.

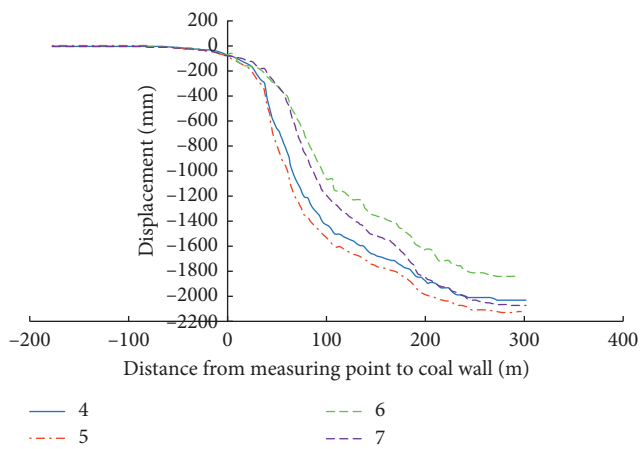

Figure 19: The displacement curves of the overlying strata at the second measuring line.

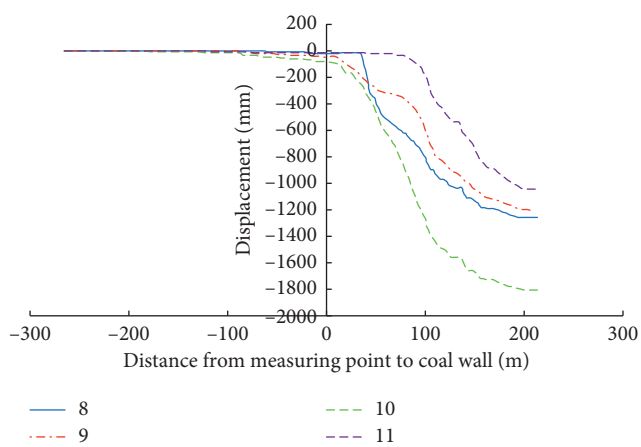

Figure 20: The displacement curves of the overlying strata at the third measuring line.

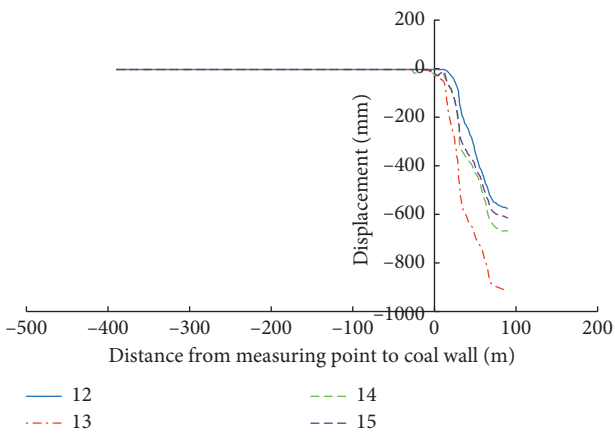

Figure 21: The displacement curves of the overlying strata at the fourth measuring line.

strata is indeed larger than that of the lower strata in some parts of the strata, and a number of obvious vertical fissures from the top to the bottom are formed on the overlying strata of the synclinal axis because of the larger dip angle and elevation angle of the strata. The entire overburden layer of the cutoff to the synclinal axis is damaged and slips along the coal seam strike toward the shaft. In addition to the vertical subsidence of the upper strata along with the lower strata, the upper strata may also slip downward along the strike of the strata. The superposition of the two displacements may cause the above phenomena.

(2) In terms of the displacement amount, the second measuring line located in the back section of the downhill mining section is the largest (the maximum cumulative displacement is more than 2000 mm), the maximum cumulative displacement of the first measuring line located in the front section of the downhill section is about 1600 mm, and the maximum cumulative displacement of the third measuring line located at the synclinal axis is about 1200 mm. Since the subsidence of the rock in the downhill mining section is not stable at the end of the experiment, the data of the fourth measuring line are not comparable.

(3) The displacement and deformation process and duration of the overlying strata are different at different locations. The overlying strata at the front of the downhill mining section (the first measuring line) basically subside at a uniform speed and tend to be stable after the working face is advanced for about 350 m. This is because the overlying strata are less affected by mining disturbance at this time, and the internal damage of the rock layer is small, so the deformation is not severe; the rock strata in the back section of the downhill mining section (the second measuring line) enter the stage of severe deformation after advancing about 30–50 m. After advancing about 200 m, the deformation slows down and the cumulative displacement tends to be stable. The strata in the synclinal axis (the third measuring line) enter the stage of severe deformation after advancing about 30–80 m on the working face. After the working surface is advanced over about 160 m, the deformation is slowed down and the cumulative displacement tends to be stable.

(4) When the working face has not been advanced to the observation line, the influence of the preabutment pressure on the activity of the overlying strata is also different in each section. The analysis of this phenomenon is of great significance to the advance support of the roadway. The influence of the advancing support pressure on the rock strata activity in the latter part of the downhill mining section (the second measuring line) is obvious. The rock layer has a displacement of about 60 mm; the influence of the other measuring lines on the preabutment pressure is not obvious.

4. Conclusion

According to the geological conditions and lithologic parameters of the E1108 working face, a physical similarity model was established. The distribution law of abutment pressure, movement law, and distribution range of water-conducting fracture zone after mining are analyzed emphatically. The analysis results show the following:

(1) The immediate roof of the downhill mining section is not easy to cave under the influence of the pressure along the layer, and the collapse drawing pace is longer; the uphill mining section is affected by the tensile force along the layer, and the collapse drawing pace is shorter, basically falls with the mining. The old roof presents different collapsing characteristics in the downhill mining section, the syncline axis, and the uphill mining section.

(2) In the process of mining, the development of the separation layer fissures and vertical fissures of overlying strata shows a certain regularity. The vertical fissures are most obvious at the boundary of goaf and the syncline axis, and the degree of the fissure development is the highest.

(3) In the preabutment pressure of the working face, the area of the syncline axis is the largest, and the downhill mining section is the smallest. Since the pressure cell is arranged in the rock layer above the coal seam, the peak value of the preabutment pressure observed is hysteresis, which all appear after mining.

(4) Through the observation and analysis of the displacement of the overlying strata, it is found that the overall subsidence phenomenon exists in the overlying strata, the cumulative displacement of the overlying strata is the largest in the downhill mining section at different stages, and the displacement and deformation processes and duration of the overlying strata are different at different locations.

(5) Based on the analysis of three zones of overlying strata, the scope of caving zone and fracture zone is

determined, the scope of water-conducting fissures in overlying strata is further determined, and the danger of water permeability in each stratum is analyzed, which provides a basis for water prevention and control.

Data Availability

(1) The data used to support the findings of this study are included within the article. And all data are obtained through experiment and test by our research team in Xinji No. 2 coal mine and laboratory. (2) All the data are true and effective. (3) The right to using data belongs to the authors before the article being published, but after it was published, the data can be referenced.

Conflicts of Interest

The authors declare no conflicts of interest.

Acknowledgments

This paper was supported by "2014 Shanxi Province Coal Based Key Scientific and Technological Projects (MJ2014-12)," "Priority Academic Program Development of Jiangsu Higher Education Institutions," and "the Fundamental Research Funds for the Central Universities (2017XKQY044)".

References

[1] H. Xie, S. Peng, and M. He, *Deep Mining Basic Theory and Engineering Practice*, pp. 3–32, Science Press, Beijing, China, 2005.

[2] M. He, H. Xie, S. Peng et al., "Study on rock mechanics in deep mining engineering," *Chinese Journal of Rock Mechanics and Engineering*, vol. 24, no. 16, pp. 2803–2813, 2005.

[3] M. Qian, *Strata Control and Sustainable Coal Mining*, China University of Mining and Technology Press, Xuzhou, China, 2011.

[4] M. Qian, F. He, Q. Li et al., "Roof control in "tip to face" area of a fully mechanized longwall face," *Coal Scienceand Technology*, vol. 21, no. 1, pp. 41–46, 1992.

[5] M. Qian, X. Miao, J. Xu et al., *Study of Key Strata Theory in Ground Control*, China University of Mining and Technology Press, Xuzhou, China, 2003.

[6] Y. Wu, D. Yun, and B. Zhou, "Study on the elementary problems of full-mechanized coal mining in greater pitching seam," *Journal of China Coal Society*, vol. 25, no. 5, pp. 465–468, 2000.

[7] Y. Wu, P. Xie, D. Yun et al., "Theory and practice of fully mechanized longwall mining in steeply dipping coal seams," *Mining Engineering*, vol. 65, no. 1, pp. 35–41, 2013.

[8] Y. Zhao, X. Zhang, and M. Tu, "Roof caving characteristic and strata behavior in exploiting steep coal seams," *Journal of Mining and Safety Engineering*, vol. 24, no. 2, pp. 231–234, 2007.

[9] G. Yin, X. Xian, G. Dai et al., "Basic behaviors of strata movement in seam with deep dip angle," *Chinese Journal of Geotechnical Engineering*, vol. 23, no. 4, pp. 450–453, 2001.

[10] W. Li, Z. Wan, F. Jiang et al., "Numerical simulation of head top coal' s stability control of fully mechanized long-wall mining with sublevel caving face in large dip seam," *Journal of China University of Mining and Technology*, vol. 37, no. 6, pp. 797–801, 2008.

[11] Y. Yuan, S. Tu, F. Dou et al., "Support instability mechanism of fully mechanized top coal caving face with steep coal seams and its control," *Journal of Mining and Safety Engineering*, vol. 25, no. 4, pp. 430–434, 2008.

[12] Y. V. Bondarenko, A. Y. Makeev, P. Zhurek, and L. Klega, "Technology of coal extraction from steep seam in the OstravaKarvina basin," *Ugol Ukrainy*, no. 3, pp. 45–48, 1993.

[13] V. N. Kulakov, "Geomechanical conditions of mining steep coal beds," *Journal of Mining Science*, vol. 31, no. 7, pp. 136–143, 1995.

[14] R. B. Mathur, D. K. Jain, and B. Prasad, "Extraction of thick and steep coal seams- a global overview," in *Proceedings of 4th Asian Mining Conference on Exploration, Exploitation, Environment*, pp. 475–488, Calcutta, India, 1993.

[15] J. M. Ongallo Acedo, A. Femandez Villa, and J. L. Lglesias Alvarez, "Experience with integrated exploition systems in narrow, very steep seams in HUNOSA," in *Proceedings of 8th International Congress on Mining and Metalurgy*, pp. 16–22, San Diego, CA, USA, October 1998.

[16] J. Bodi, "Safety and technological aspects of manless exploitation technology for steep coal seams," in *Proceedings of 27th International Conference of Safety in Mines Research Institutes*, pp. 955–965, New Delhi, India, February 1997.

[17] V. N. Kulakov, "Stress state in the face region of a steep coal bed," *Journal of Mining Science*, vol. 31, no. 9, pp. 161–168, 1995.

[18] S. Ping and W. Li, "Strata pressure appearance around roadway during combined coal mining in steep inclined seam with small space between seams," *Coal Science and Technology*, vol. 10, pp. 2–6, 1994.

[19] L. Tao and Y. Wang, "Movement and failure of overlyings tratain a face in steep seam," *Journal of the China Coal Society*, vol. 11, pp. 582–585, 1996.

[20] Y.-p. Wu, P.-s. Xie, S.-g. Ren, and R.-b. Li, "Three-dimensional strata movement around coal face of steeply dipping seam group," *Journal of Coal Science and Engineering (China)*, vol. 14, no. 3, pp. 352–355, 2008.

[21] G.-f. Wang, "New development of longwall mining equipment based on automation and intelligent technology for thin seam coal," *Journal of Coal Science and Engineering (China)*, vol. 19, no. 1, pp. 97–103, 2013.

[22] P. Xie, Y. Wu, H. Wang et al., "Stability analysis of incline masonry structure and support around longwall mining face area in steeply dipping seam," *Journal of China Coal Society*, vol. 37, no. 8, pp. 1275–1280, 2012.

[23] C. Su, P. Gou, and G. Deng, "Testing equipment development of mining similar model on biaxial stress," *Journal of Henan Polytechnic University*, vol. 26, no. 2, pp. 141–145, 2007.

[24] C. Liu, Y. Guo, and J. Yao, "The development and problems of mining similar simulation experiment technique," *China Mining Magazine*, vol. 12, no. 8, pp. 6–8, 2003.

[25] X. Jiang, X. Jiang, and J. Chen, "New method to determine the main roof pressure in tridimensional simulated test," *Ground Pressure and Strata Control*, vol. 19, no. 4, pp. 81-82, 2002.

[26] S. Li, D. Wang, Q. Wang et al., "Development and application of large-scale geomechanical model test system for deep thick top coal roadway," *Journal of China Coal Society*, vol. 38, no. 9, pp. 1522–1530, 2013.

[27] A. Chen, J. Gu, and J. Shen, "Development and application of multifunctional apparatus for geotechnical engineering model tests," *Chinese Journal of Rock Mechanics and Engineering*, vol. 23, no. 3, pp. 372–378, 2004.